ChemPhysChem

Research Article
doi.org/10.1002/cphc.202300214

Chemistry Europe
European Chemical Societies Publishing

www.chemphyschem.org

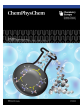

Production of Dihydrogen Using Ammonia Borane as Reagent and Pyrazole as Catalyst

Marta Delgado Gómez,[a] Marco Marazzi,*[a, b] José Elguero,[c] Maxime Ferrer,[c, d] and Ibon Alkorta*[c]

Theoretical chemistry (DLPNO-CCSD(T)/def2-TZVP//M06-2x/aug-cc-pVDZ) was used to design a system based on ammonia boranes catalyzed by pyrazoles with the aim of producing dihydrogen, nowadays of high interest as clean fuel. The reactivity of ammonia borane and cyclotriborazane were investigated, including catalytic activation through 1*H*-pyrazole, 4-methoxy-1*H*-pyrazole, and 4-nitro-1*H*-pyrazole. The results point toward a catalytic cycle by which, at the same time, ammonia borane can initially store and then, through catalysis, produce dihydrogen and amino borane. Subsequently, amino borane can trimerize to form cyclotriborazane that, in presence of the same catalyst, can also produce dihydrogen. This study proposes therefore a consistent progress in using environmentally sustainable (metal free) catalysts to efficiently extract dihydrogen from small B–N bonded molecules.

Introduction

Materials capable of storing hydrogen are a possible alternative to hydrocarbon-based fuels, since they are more environmentally friendly sources of energy and could help improving the environmental situation.[1] According to the literature, molecules with B–N bonds are interesting systems for hydrogen storage,[2] and that is why we have computationally studied the reaction involving ammonia borane **1** (BNH_6) and cyclotriborazane **4** ($B_3N_3H_{12}$) as reagents with pyrazole **6** acting as catalyst. These and related molecules are shown in Figure 1.

Especially, on one hand, ammonia borane **1** and amino borane **2** are single and double B–N bonded molecules, isoelectronic with ethane and ethene, respectively, while cyclotriborazane **4** and borazine **5** are isoelectronic with cyclohexane and benzene, respectively. Imido borane **3** (BNH_2), on the other hand, contains a triple B–N bond being isoelectronic with acetylene and, even though it has been characterized by laser spectroscopy,[3] it is highly reactive and it spontaneously trimerizes to form borazine **5**.[4]

Boron, with electronic configuration [He] $2s^2$ $2p^1$, has empty p orbitals making it a potential electron acceptor when trying to complete its valence shell. Nitrogen, with electronic configuration [He] $2s^2$ $2p^3$, has three unpaired electrons in three p orbitals and usually acts as electron donor.

As a result, **1** is a neutral system in which both boron and nitrogen are sp^3 hybridized, with the B–N dative bond originated by the nitrogen atom sharing a pair of electrons (N:→B).[5] **1** is considered an important material in hydrogen storage thanks to its high stability, even at high temperatures (melting point 102 °C), and its important hydrogen storage capacity, 19.6 % by weight of H_2.[6] At temperatures up to 100 °C, solid **1** is capable of providing a single equivalent of H_2 and, as byproducts, amino borane oligomers, $[-H_2B-NH_2-]_n$.[6] It has been found that the main characteristic of ammonia borane crystals are their polar $N-H^{\delta+}\cdots{}^{-\delta}H-B$ dihydrogen bonds[7] between monomers. Furthermore, it has been shown that the presence of these polar dihydrogen bonds between monomers, as well as other non-covalent interactions, not only results in chemical stability but can also facilitate various dehydrogenation steps.[8]

The dehydrogenation steps require, nevertheless, a catalytic activation to finally release H_2 from **1**, as described in the literature, usually by the use of metal complexes: Guan et al.[9] and Agapie et al.[10] in 2014 attempted to catalyze the reaction by iron and molybdenum complexes, then Williams et al.[11] in 2016 used a ruthenium complex, while Shubina et al.[12] in 2018 employed an iridium complex (**7** in Scheme 1) transforming **1** into compounds **8** and **4** with concomitant production of dihydrogen.

More recently, in 2021, Garralda et al. proved that (acylquinoline)(−norbornenyl)(pyrazole) Rh(III) complexes are efficient catalysts for the hydrolysis of **1** while reacting with $PPh_2(O)$ in air to release dihydrogen.[13]

[a] *M. Delgado Gómez, Dr. M. Marazzi*
Universidad de Alcalá, Departamento de Química Analítica, Química Física e Ingeniería Química, Ctra. Madrid-Barcelona, Km 33,600, 28871 Alcalá de Henares, Madrid, Spain
E-mail: marco.marazzi@uah.es
[b] *Dr. M. Marazzi*
Universidad de Alcalá, Instituto de Investigación Química "Andrés M. del Río" (IQAR), 28871 Alcalá de Henares, Madrid, Spain
[c] *Prof. J. Elguero, M. Ferrer, Prof. I. Alkorta*
Instituto de Química Médica CSIC, Juan de la Cierva, 3, 28006 Madrid, Spain
E-mail: ibon@iqm.csic.es
Homepage: http://are.iqm.csic.es
[d] *M. Ferrer*
PhD Program in Theoretical Chemistry and Computational Modeling, Doctoral School, Universidad Autónoma de Madrid, 28049 Madrid, Spain

Supporting information for this article is available on the WWW under https://doi.org/10.1002/cphc.202300214

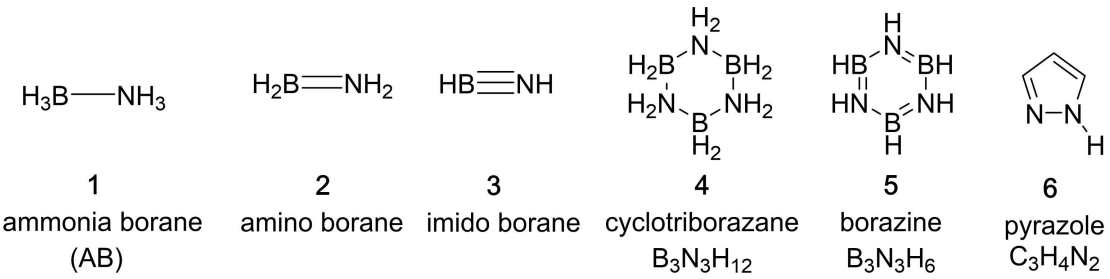

Figure 1. B–N bonded systems (**1**–**5**) suggested for hydrogen storage. In this study, **1** and **4** are proposed as reactants, catalyzed by **6**, to produce dihydrogen.

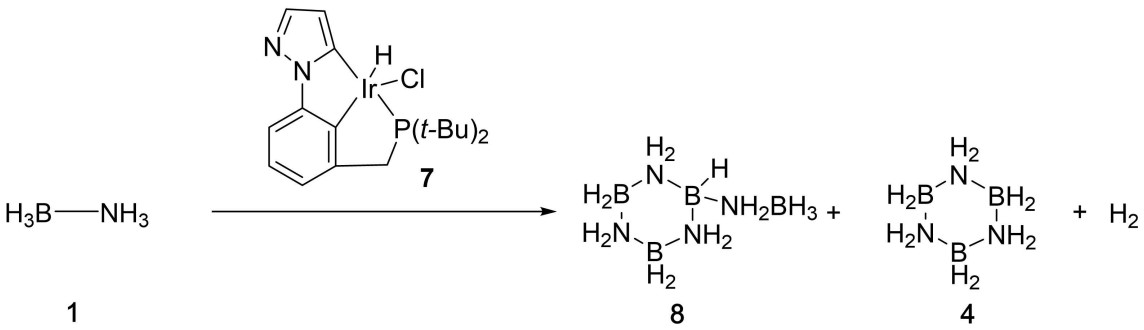

Scheme 1. Iridium complex **7** shown to act as a catalyst to dehydrogenate ammonia borane, while forming cyclotriborazane **4** and its derivative **8** as byproducts.

Although such transition metal-based catalysts have therefore shown encouraging results, it has to be noted their high cost production and relatively poor sustainability for the environment. Metal-free organic-based compounds would, on the other hand, largely solve both problems, if they could act as efficient dehydrogenation catalysts. Indeed, Baker et al.[14] first in 2007, and Wegner et al.[15] later in 2015 proposed fully organic catalysts that can release ca. 2.5 equivalents of H_2, similarly to some metal-based counterparts. More recently (2020), Gellrich et al. described that 6-*t*-butyl-2-thiopyridone, thanks to the catalytic activity of the basic pyridone ring and the steric requirement of the *t*-butyl group, could be potentially used as a catalyst for **1** dehydrogenation.[16]

Inspired by this idea, here we propose pyrazole **6** as a catalyst (Scheme 2). In addition, the reaction of cyclotriborazane, **4**, to yield borazine and three H_2 molecules has also been considered. The potential influence of the substituents in the pyrazoles has been taken into account by studying the reactions with the 4-nitro and 4-methoxypyrazole derivatives. Finally, the solvent effect has been analyzed. In all these cases, all the stationary points (minima and transition states, TSs) connecting the reactants and final products have been characterized using M06-2X/aug-cc-pVDZ DFT methods. Based on these results, the kinetic of the reactions have been calculated through transition state theory.

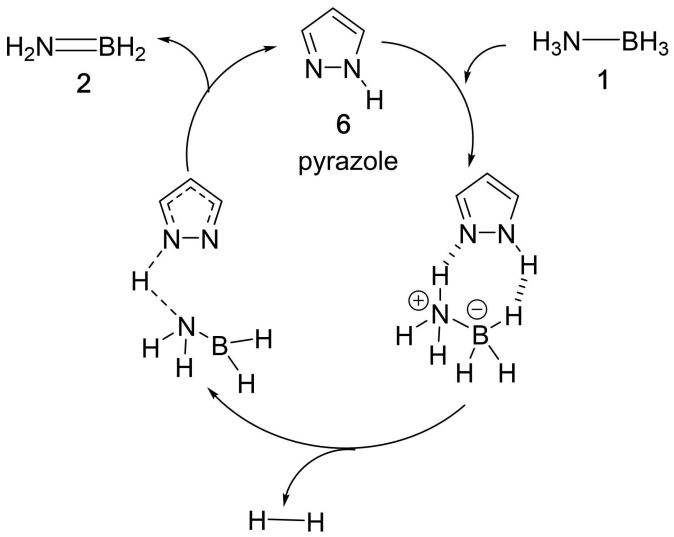

Scheme 2. Catalytic reaction proposed to produce H_2 using ammonia borane as reagent and pyrazole as catalyst. Amino borane is also obtained as byproduct.

Computational Details

Geometry optimizations were carried out with Density Functional Theory (DFT) by using the M06-2X DFT functional[17] with the aug-cc-pVDZ basis set,[18] as implemented in the scientific software Gaussian16.[19] This specific hybrid functional was chosen since, among the Minnesota ones, it was developed to perform better for weakly correlated systems. Moreover, the use of the M06-2X functional together with a highly converged basis set was

demonstrated to be a suitable computational strategy to study different ammonia borane reactivities.[20] Frequency calculations of all optimized geometries were carried out at the M06-2X/aug-cc-pVDZ level of theory, confirming the nature of the located stationary points: energy minima (no imaginary frequencies) or TSs (only one imaginary frequency). In order to improve the energetic description of the stationary points, the domain-based local pair natural orbital coupled-cluster theory (DLPNO-CCSD(T))[21] method was used by single point DLPNO-CCSD(T)/def2-TZVP calculations on top of the DFT optimized geometries, using the Resolution of Identity (RI) approximation for Coulomb (J) and HF exchange (K) integrals (resulting in the RI-JK approximation), along with the def2-TZVP/C and def2/JK auxiliary basis sets, using the tightPNO option as implemented in the Orca5 program.[22] This methodology provides similar results to those obtained with the standard CCSD(T) method, but significantly decreasing the computational cost.[23] The resulting energies incorporate the DLPNO electronic energy and the thermal corrections at M06-2X level.

The geometries of the stationary points (minima and TSs) have been gathered in Table S1 of the Supporting Information Material.

The solvent effect on the reaction profile has been calculated by means of Integral Equation Formalism-Polarizable Continuum Model (IEF-PCM).[24] Especially, tetrahydrofuran (THF) was selected as solvent, as it was used for previous experiments.[16]

The electron density has been analyzed with the Quantum Theory of Atoms In Molecules (QTAIM),[25] using the AIMAll program.[26] The presence of (3,–1) critical points, known as bond critical points (bcp), associated to interatomic interactions and its properties allows to classify such contacts as covalent or non-covalent.[27] Covalent interactions are characterized by large values of the electron density at the bcp with negative values of the Laplacian and total energy density. Weak interactions show small values of the electron density at the bcp, with positive values of the Laplacian and the energy density. Medium interactions show positive values of the Laplacian but negative values of the energy density and strong non-covalent interactions present similar electron density properties to the ones found in covalent bonds (negative Laplacian and energy density).

Results and Discussion

The mechanism proposed in this work to produce hydrogen is based on the dehydrogenating of borazanes (compounds already suggested for hydrogen storage purposes) catalyzed by pyrazole (Scheme 2). It should be noted that pyrazole presents acid-base properties due to a basic center (N moiety with a lone pair capable of accepting a proton) and an acid center (NH moiety capable of donating a proton).[28]

Due to these pyrazole properties, we propose a mechanism composed of two initial simultaneous steps: the proton of the NH group of the pyrazole interacts with the hydride B–H of **1**, allowing H_2 release and, at the same time, one of the NH groups of **1** interacts with the N moiety of the catalyst, producing a proton transfer that forms **2** (BNH_4) as byproduct. Finally, the catalyst can be recovered after a prototropic tautomerism between the nitrogen atoms of the pyrazole.

Once the feasibility of the mechanism was verified, we studied the effect of the substituents in position 4 of the pyrazole (4-NO_2 and 4-OCH_3) and the effect of the solvent, to analyze how these variables affected the proposed reaction.

In the nomenclature used along the article, the "+" sign indicates the sum of the energies of the isolated reactant and catalyst, while ":" corresponds to their energy when forming a complex. For instance, "**6**+**1**" corresponds to the sum of the energy of the isolated pyrazole and ammonia borane in their minimum energy configuration, while "**6:1**" refers to the formed complex between **6** and **1**.

Main reaction

The main reaction is represented in Scheme 3. The energetic profiles of Figure 2 and the geometries of the stationary points shown in Figure 3, correspond to this Scheme.

The energetic profiles presented in Figure 2 show important differences between the ones of free energy and the ones of the electronic and enthalpy energies. This is due to the large entropic contribution when the number of molecules changes during the reaction. In the first step, i.e., **6**+**1** (two molecules) to **6:1** (one supramolecular assembly, or supermolecule), the reduction in the number of isolated particles causes a change of $-51.5\ kJ\cdot mol^{-1}$ in relative enthalpy, and of $-9.1\ kJ\cdot mol^{-1}$ in relative free energy: a $-42.2\ kJ\cdot mol^{-1}$ difference. In the last step (the fourth one), i.e., **6:2**:H_2 (one supermolecule) to **6**+**2**+H_2 (three separated molecules), H_2 is finally released and the catalyst is regenerated, hence resulting in an increase of the number of isolated particles that causes the enthalpy to decrease by $-2.8\ kJ\cdot mol^{-1}$, while the free energy decrease by $-57.3\ kJ\cdot mol^{-1}$: a $+60.1\ kJ\cdot mol^{-1}$ difference. Concerning the transition state formation (TS, second step) there is no change in the number of particles, kept to one, with $\Delta H = +117.8\ kJ\cdot mol^{-1}$ and $\Delta G = +123.6\ kJ\cdot mol^{-1}$: a much lower $+5.8\ kJ\cdot mol^{-1}$ difference, compared to the aforementioned steps.

It has to be noted that the global reaction is, in the thermodynamic point of view, largely exergonic, *i.e.* spontaneous ($\Delta G < 0$), although a relatively significant energy barrier should make it kinetically slow. In the technological point of view, this could be actually positive, since dihydrogen could be released in a controlled fashion, possibly at demand. Especially, according to transition state theory,[29] at room temperature the

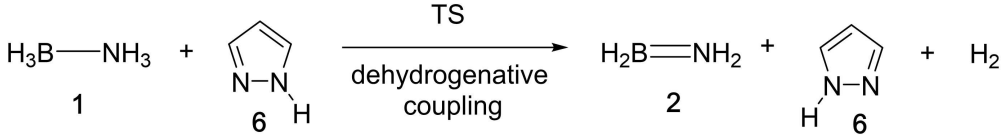

Scheme 3. Overall chemical reaction indicating the production of dihydrogen from **1** catalyzed by pyrazole.

Research Article
doi.org/10.1002/cphc.202300214

Chemistry Europe
European Chemical Societies Publishing

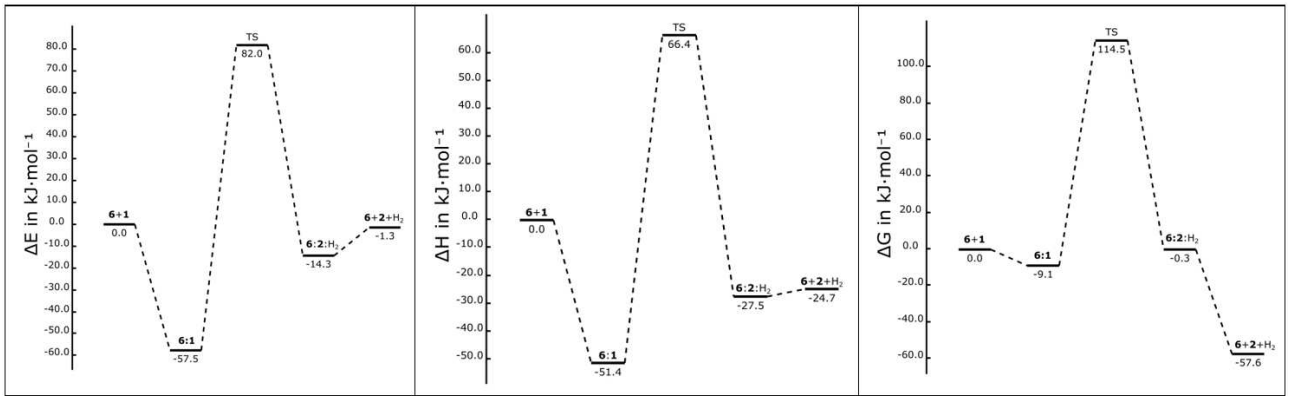

Figure 2. Electronic (left), enthalpy (center) and free energy (right, at 298 K) profiles, in kJ·mol^{-1}, including DLPNO corrections following Scheme 3.

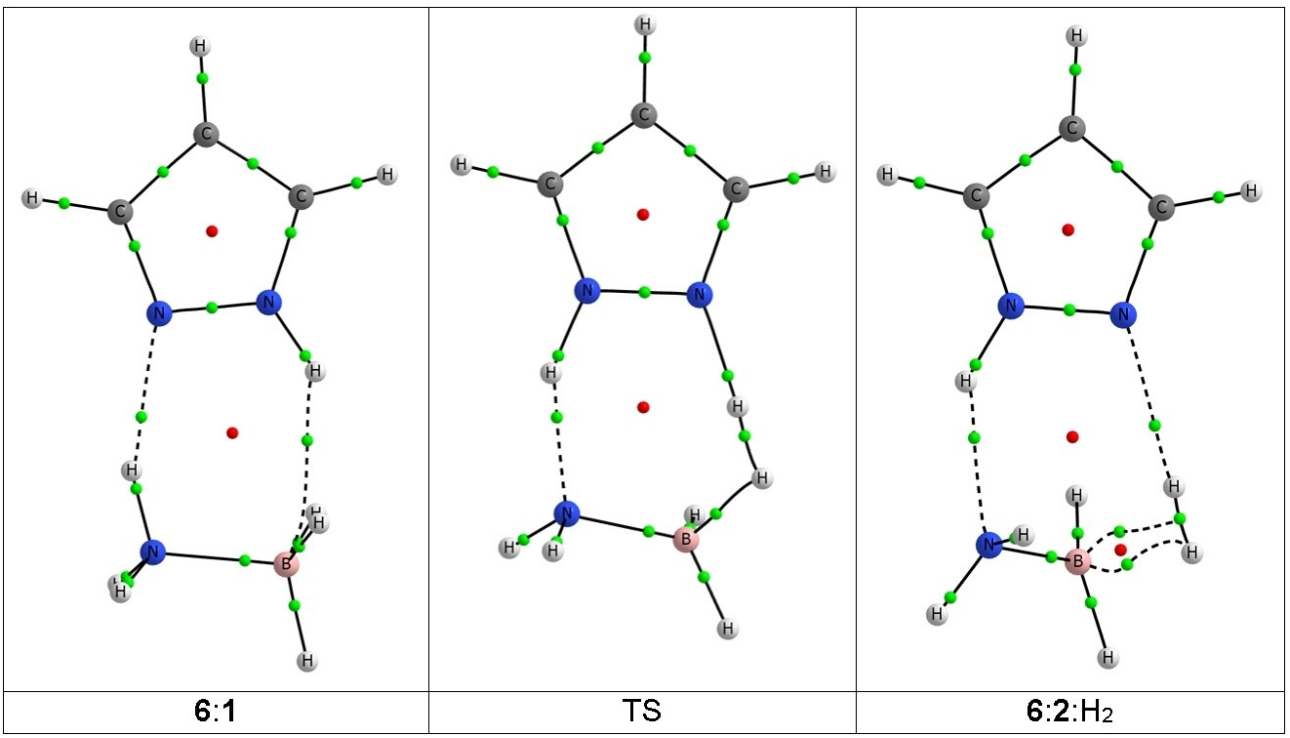

Figure 3. Molecular graph of the stationary points from Figure 2. Green and red small spheres identify the location of the bond and ring critical points, respectively.

velocity constant k for this reaction is estimated to be $1.38 \cdot 10^{-9}\ s^{-1}$, resulting in an expected high lifetime τ(r.t.) = $8.36 \cdot 10^{3}$ days. By properly heating the reaction mixture, we can *ad hoc* favor the dihydrogen release: at mild conditions, τ(70 °C) = 10.5 days, and increasing more the temperature we could reach almost immediate H_2 release: τ(150 °C) = 3.40 minutes.

The molecular graph representations (including bond paths, bond and ring critical points, belonging to QTAIM) of the most interesting stationary points (**6:1**, **TS**, and **6:2**:H_2) involved in the reaction are shown in Figure 3. The pre-reactive complex, **6:1**, shows two simultaneous interactions of the acid and basic moieties of the pyrazole with the complementary ones of **1**. The analysis of the electron density shows the presence of intermolecular bond critical points (bcp). Its properties are typical of weak non-covalent interactions:[27] small values of ϱ_{bcp} (0.030 and 0.015 a.u. for the N···H and H···B contacts) and positive values of the Laplacian, $\nabla^2\varrho_{bcp}$, in both cases (Table S1). These two simultaneous interactions explain the stabilization found in the **6:1** complex (−57.5 kJ·mol^{-1}) with respect to **6** + **1**. In the TS structure, the proton from the NH group of **1** is already transferred to the pyrazole. The formation of an incipient H_2 molecule with an interatomic distance of 0.94 Å is due to an elongation of the pyrazoles N–H and **1**'s B–H bonds

(1.41 and 1.34 Å, respectively). Both such bonds involved in the formation of H_2 show smaller values of the ϱ_{bcp} (0.115 and 0.100 a.u., respectively) than in the complex, while H_2 shows increasing characteristics of covalent bond with a value of ϱ_{bcp} of 0.155 a.u. and a negative value of the Laplacian. The resulting **6:1**:H_2 product complex shows a H_2 molecule with an interatomic distance slightly larger (0.80 Å) than when isolated (0.76 Å) due to the simultaneous interaction with one of the nitrogen atoms of the pyrazole and the boron atom of **1**. The ϱ_{bcp} of the H_2 molecule increases up to 0.235 a.u., very close to the one found in the isolated molecule (0.253 a.u.).

Effect of pyrazole substitution patterns on the main reaction

To estimate how the acidity and basicity of the substituents on the pyrazole ring can influence H_2 production, we have selected the electron donor 4-methoxy group and the electron acceptor 4-nitro group (**9** and **10** in Figure 4), with the goal of decreasing and increasing the acidity, respectively. Acid/base properties of pyrazoles have been shown in the literature to be linearly related, following the empiric relation: $pK_a = 11.04 + 0.916\ pK_b$.[30]

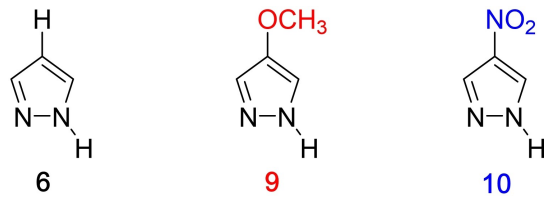

Figure 4. Pyrazole (**6**) and its two derivatives studied in this work.

Figure 5 shows the energetic profile of the reaction to produce H_2 for the parent pyrazole and for the two (4-methoxy and 4-nitro) derivatives considered.

The effect of the substitution on the position 4 of the pyrazole has little consequences on the energetics of the reaction: the formation of the initial complex with **1** is obtained in all cases, with a difference of less than 1.7 $kJ \cdot mol^{-1}$ with respect to **6:1**. Concerning the energy barrier determined by the transition state, the path determined by **9** results in a slight barrier reduction ($-1.2\ kJ \cdot mol^{-1}$) with an according slight decrease of the reactants lifetime (τ(r.t.) $= 5.15 \cdot 10^3$ days), and the path involving **10** in a minimal barrier raise ($+0.7\ kJ \cdot mol^{-1}$) with an according increase in lifetime (τ(r.t.) $= 1.11 \cdot 10^4$ days), compared to un-substituted **6**.

In any case, the geometries of the stationary points are affected by the pyrazole substituents (Table S2): in the pre-reactive complex the pyrazoles intermolecular N···H distance is elongated by 0.08 Å in the 4-nitro derivative with respect to the parent system, while the BH···H distance is shortened by 0.06 Å. In the TS, the interatomic distance in the incipient H_2 molecule of the parent pyrazole is 0.94 Å while in the 4-nitro derivative this distance is shorter (0.89 Å), hence indicating that the TS is closer to the products. These parameters are almost identical when considering the parent (**6**) and the 4-OCH_3 derivatives (**9**).

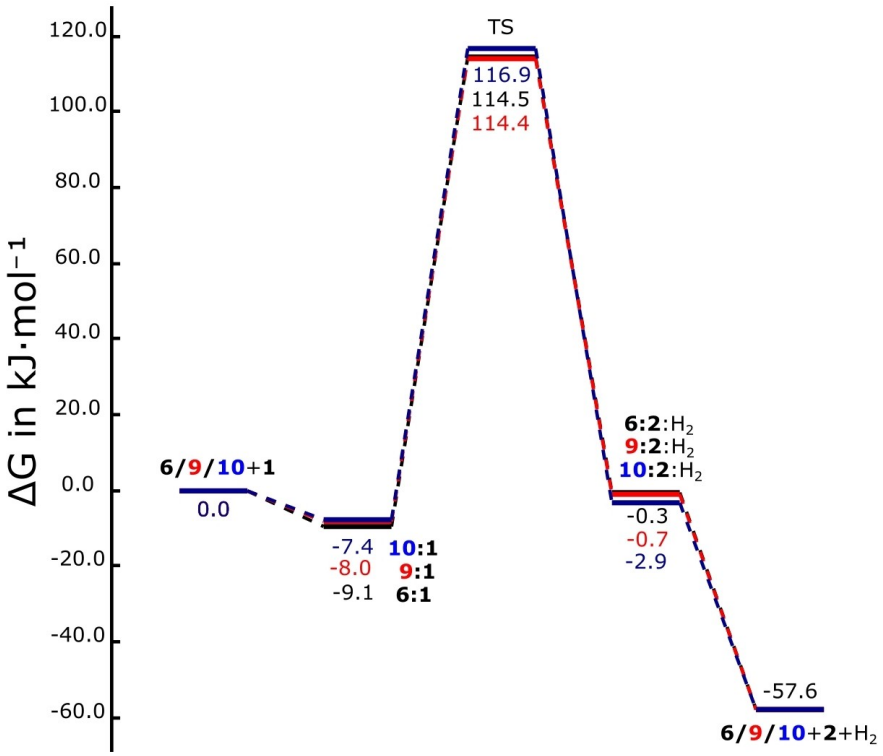

Figure 5. Free energy (at 298 K) profile of the H_2 production reaction, including the effect of the substituent on the pyrazole **6** (black), resulting in the derivatives 4-methoxypyrazole **9** (red) and 4-nitropyrazole **10** (blue). The corresponding electronic energy profile is given in Figure S1.

Reaction using cyclotriborazane 4

As shown in Scheme 2, during the catalytic dehydrogenation of **1**, **2** is obtained as a byproduct. In this section, we will show how **2** can also lead to H_2 production: as mentioned in the introduction, it is feasible to obtain a trimeric structure of **2**, cyclotriborazane **4**.[31] Once **4** is formed, by using again pyrazole as catalyst, dehydrogenation can be accomplished, in principle doubling the H_2 production yield. When comparing the X-ray structure of **4** with the one computationally optimized, we note their resemblance due to a chair conformation[32] and a dipole moment of 3.8 Debye (experimental: 3.2 Debye).[33]

The dehydrogenation reaction path of **4** to yield **5** and three molecules of dihydrogen, catalyzed by pyrazole **6**, is shown in Scheme 4 and, more in detail, in Scheme 5.

The proposed mechanism corresponds to a cascade reaction. The corresponding energy profile is depicted in Figure 6 and those involving **9** and **10** are gathered in Figure S1. Due to the similarity of the three profiles, only the one of the parent pyrazole, **6**, will be discussed here. The release of the first H_2 molecule, through TS1, is the less energetically favorable, due to a larger barrier compared to H_2 extraction from **1** (178.9 compared to 123.6 kJ·mol^{-1}) and being an endergonic process (**6**:**11**:H_2 is 22.0 kJ·mol^{-1} higher in energy than **6**+**4**). Nevertheless, the release of the second H_2 molecule, through TS2, shows an almost identical barrier (123.3 kJ·mol^{-1}) compared to H_2 extraction from **1** together with a slightly exergonic process. Even better, the release of the third H_2 molecule is highly favorable from both kinetic (57.4 kJ·mol^{-1}) and especially thermodynamic ($\Delta G = -188.8$ kJ·mol^{-1}) points of view and could be the driving force for the reaction to evolve. This last step corresponds to the formation of borazine **5**, i.e., an aromatic compound,[34] thanks to three subsequent dehydrogenation steps transforming saturated **4** into unsaturated **11**, then **12**, and finally **5**. Experimentally, **4** can be regenerated by reduction of **5**.[35]

The estimation of the kinetic parameters helps in understanding the proposed three consecutive steps, in terms of lifetime of the different species: τ(r.t.) goes from $4.08 \cdot 10^{13}$ days, calculated for the first step (i.e., the bottleneck), to $7.41 \cdot 10^{3}$ days for the second step (of the same order of magnitude as for the main reaction involving **1**), finally reaching $1.82 \cdot 10^{-3}$ seconds for the last step, hence corresponding to a barrier that can be almost instantaneously overcome. As when discussing the main reaction, also here heating the reaction flask can result in proper decrease of the reaction lifetimes. Nevertheless, in this case the relatively high barrier of the first step would require heating until 250 °C to obtain a lifetime below one day (τ(250 °C) = 18.5 hours), reaching the sub-second scale also for the second step (see Figure S2 in the Supporting

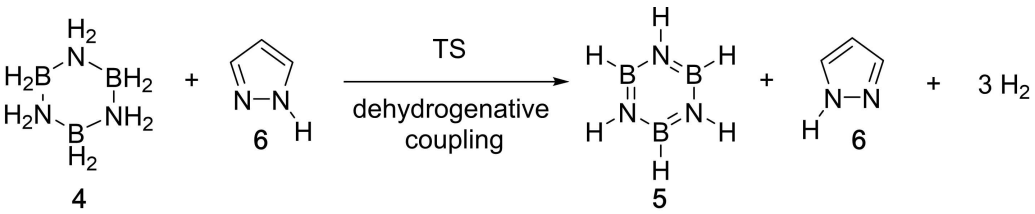

Scheme 4. Reaction of pyrazole with **4** ($B_3N_3H_{12}$).

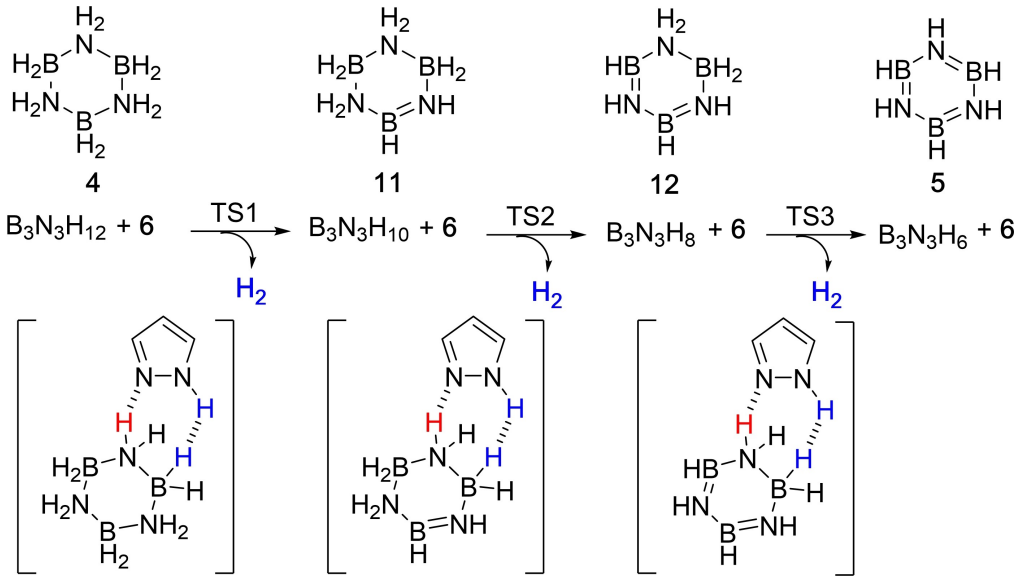

Scheme 5. Proposed mechanism for the dehydrogenation reaction of **4** using pyrazole as a catalyst.

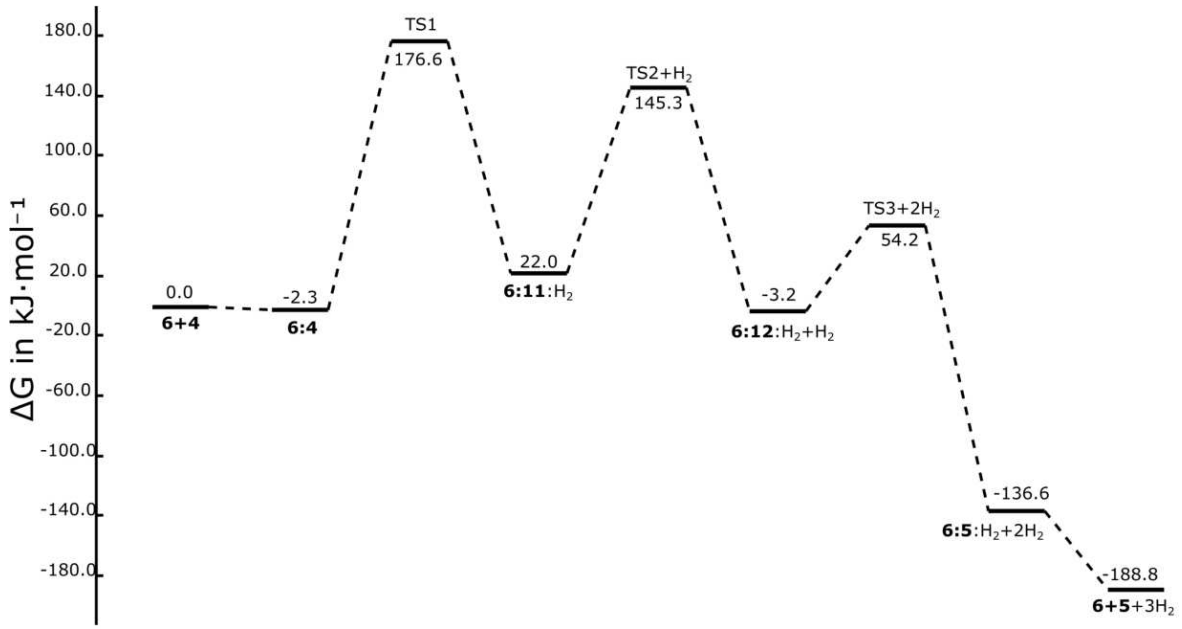

Figure 6. Free energy profile for the study of the reaction **4**→**5** + $3H_2$ catalyzed by **6**. The electronic energy profile is shown in Figure S2.

Information). Accordingly, such temperature increase would affect significantly also the expected time corresponding to the maximum concentration of the first intermediate (**6:11**:H_2), which is calculated to be $1.66 \cdot 10^5$ days at r.t., while only 23.9 s at 250 °C (see Supporting Information).

The molecular representations of the stationary points belonging to the elementary reactions of Figure 6, are shown in Figure 7. In the **6:4** and **6:11** complexes acting as reactants, bifurcated hydrogen bonds are observed, acting the N–sp^2 of the pyrazole as multiple HB acceptor stabilizing the geometries of the structures found as minima. In addition, dihydrogen bonds are noticed here as contributors of the complex's stability. In **6:12**, two H···N hydrogen bonds are obtained. The geometry of the corresponding TS3 shows a similar arrangement to the one obtained in the **6** + **1** reaction, with an elongation of the B–H and N(pyrazole)-H bonds and the formation of an incipient H_2 molecule with intermolecular distances of 0.94, 0.92 and 0.94 Å in the TS1, TS2 and TS3, respectively.

The H_2 formed in the product of each elementary reaction is involved in hydrogen bonds as donor, along the H–H axis, where the electron density is depleted and as acceptor with the σ electrons of the H–H bond.[36]

Solvent effect

To determine the effect of the solvent on the proposed mechanism, a study was carried out selecting tetrahydrofuran (THF) as implicit solvent in the **1**→**2** + H_2 reaction catalyzed by **6**, as it was previously used for this type of experiments.[16] By comparing the results obtained in gas phase and through the solvation model (Figure 8), we can observe that each step of the reaction profile in THF is higher in energy than the corresponding in gas phase. Of particular relevance is the first step, corresponding to complex formation between the reactant and the catalyst, since it becomes unfavorable when including THF, therefore already suggesting that the following steps are less likely to take place. In any case, since this first aggregation step requires 23.3 $kJ \cdot mol^{-1}$ it should be mainly driven in solution by effective collisions in order the reaction to proceed. Then, an only slightly higher energy barrier (143.2 compared to 123.6 $kJ \cdot mol^{-1}$) separates the reactant from dihydrogen production, that is finally also exergonic in THF, although to a lesser extent than in gas phase (−20.3 compared to −57.6 $kJ \cdot mol^{-1}$). These differences could be explained based on the polar character of **1**, that shows a high dipolar moment (5.3 Debye) that decreases along the reaction up to 1.8 Debye in **2**.

From the thermodynamic point of view, we should highlight that the shown energy profiles do include the formation of the light H_2 gas molecule, that is expected to rapidly leave the liquid reaction medium, thus favoring reaction evolution towards the products.

From the kinetic point of view, the increased energy barrier results in a ca. 10^4 days raise of τ(r.t.) compared to gas phase, hence requiring a temperature increase until 220 °C to reach a comparable τ(r.t.) = 2.38 minutes (see Figure S3).

The solvent effect in the rest of the reactions studied (modifying the catalyst, **9** + **1** and **10** + **1**, or modifying the reactant, **6** + **4**) also shows that they are less favorable than in gas phase, although only slightly. Their energy profiles are provided in Figure S2.

The comparison of the TS structures shows that the interatomic distance between the H atoms that will finally form H_2 are slightly longer in THF than in gas phase, while the

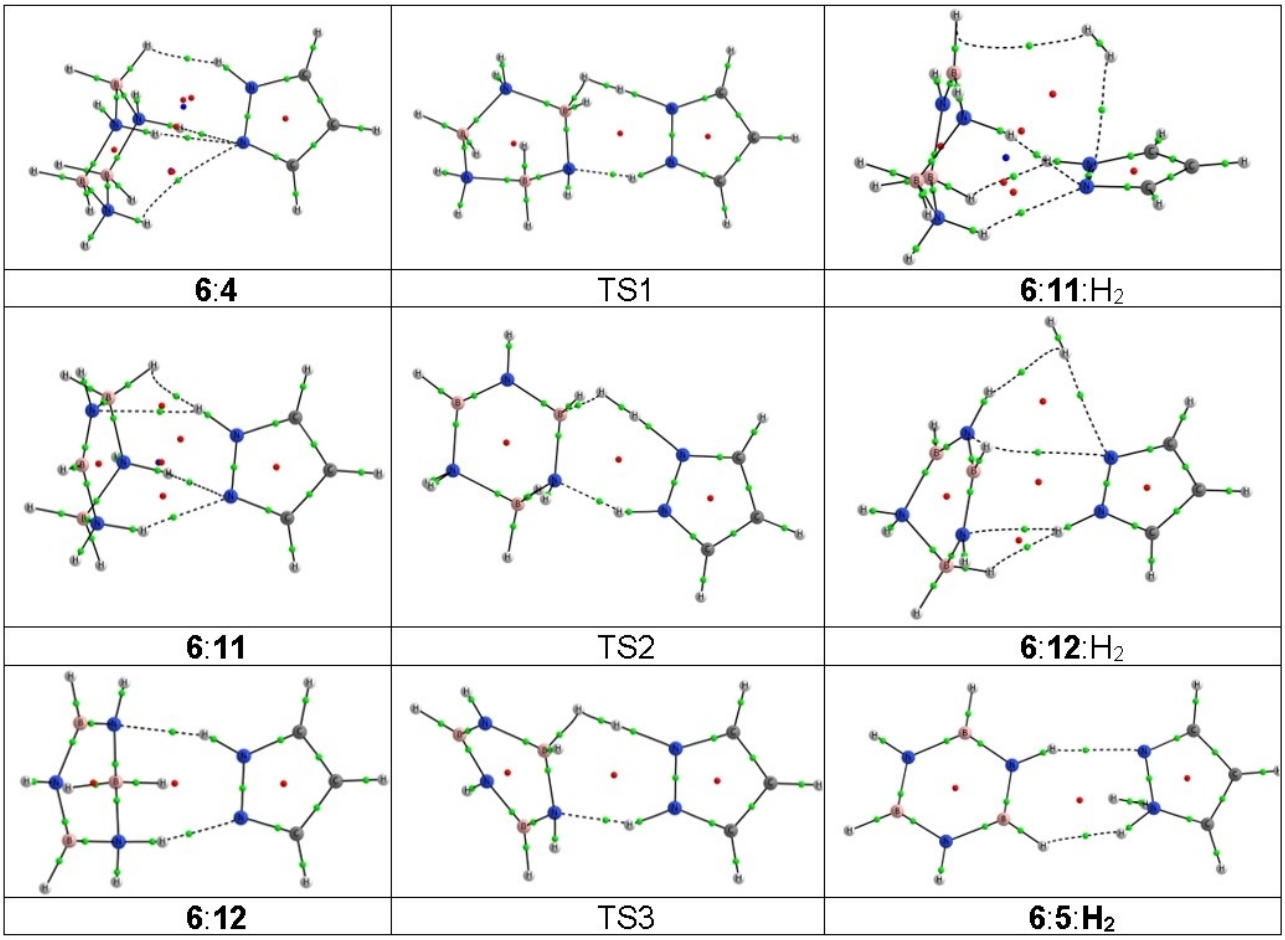

Figure 7. Molecular graph of the stationary points in the elementary reaction for the transformation of **6** + **4** in **6** + **5** + $3H_2$. The location of the bond, ring, and cage critical points are indicated with green, red, and blue small spheres, respectively.

opposite happens in the formed N–H bond in the pyrazole, that is shortened in THF than in gas phase, in this way structurally explaining the higher energy requirements when using THF.

Conclusions

We have studied a possible catalytic process involving an organic catalyst (pyrazole) for dihydrogen production from ammonia borane, already proposed to potentially store hydrogen as a physico-chemical stable compound. Interestingly, the reaction produces a single byproduct (amino borane), that is expected to trimerize spontaneously forming cyclotriborazane which, in turn, can be also catalytically activated by the same pyrazole to release dihydrogen. This could increase the dihydrogen release efficiency compared to nowadays studies, by using a metal-free sustainable compound instead of metal-based catalysts mainly proposed up to date.

In the thermodynamic point of view, all the reactions studied here are exergonic, $\Delta G < 0$. Moreover, the reaction of cyclotriborazane to release three molecules of H_2, in the presence of pyrazole as catalyst, is very exothermic due to the concomitant production of the aromatic borazine.

In the kinetic point of view, the energy barriers responsible for both **1** and **4** dehydrogenations are expected to be significantly high, resulting in high lifetimes. Nevertheless, proper heating can decrease such barriers leading to a convenient release strategy.

The substitution of pyrazole yielding a more acidic catalyst (4-nitro derivative) or a more a basic one (4-methoxy derivative) does not significantly change the energy profile of the main reaction involving ammonia borane, i.e., the first catalytic step.

Concerning solvent effects, tetrahydrofuran was selected due to solubility issues experimentally studied. The results point toward a higher energy barrier (ca. $+20\ kJ \cdot mol^{-1}$) for ammonia borane to react, compared to gas phase, although the reaction remains still feasible, also thanks to less remarkable but still evident exergonic conditions (ca. $-20\ kJ \cdot mol^{-1}$), that should drive the reaction. Thus, tetrahydrofuran or similar solvents can be considered reliable candidates to carry out experimentally the reactions explored in the present work.

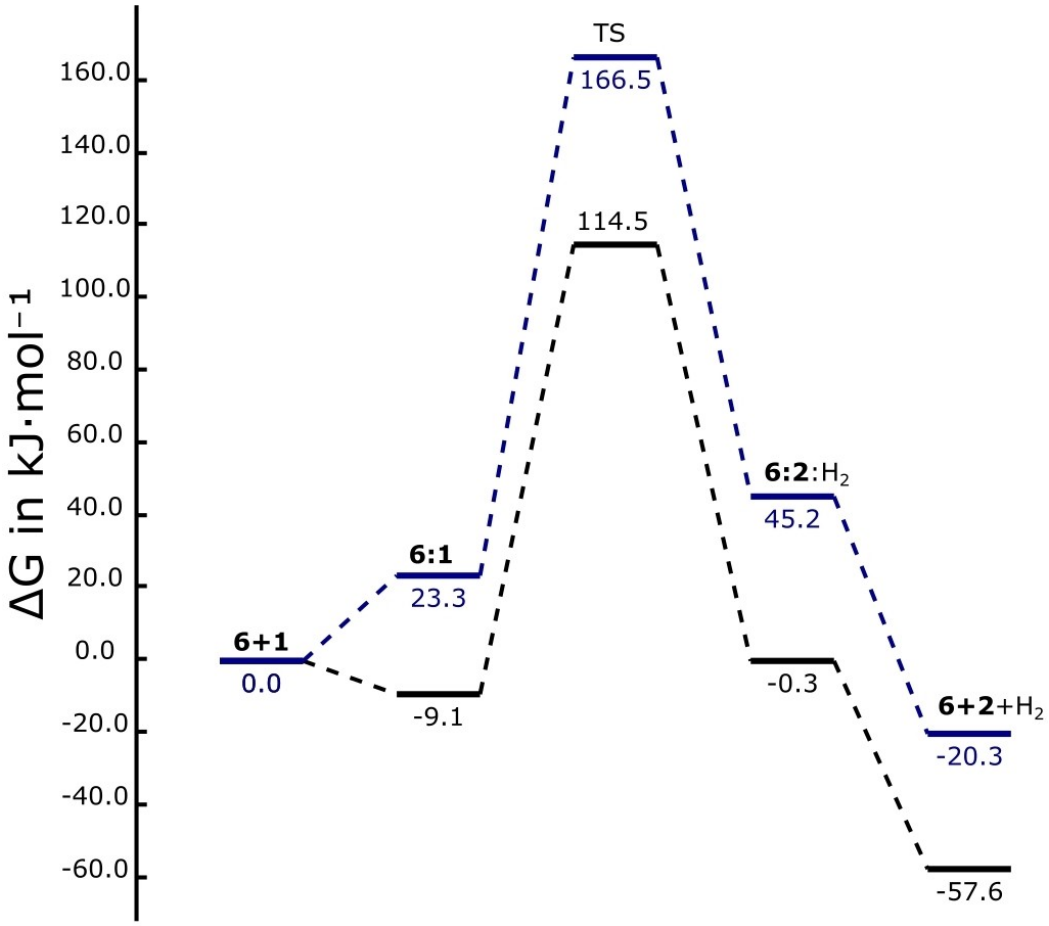

Figure 8. Free energy (at 298 K) profiles, comparing the effect of the solvent, THF (blue) with the reaction in gas phase (black) for the **1**→**2** + H_2 reaction catalyzed by **6**. The corresponding electronic energy profile is given in Figure S1.

Supplementary data

Supporting Information is available for this manuscript.

Acknowledgements

This work was carried out with financial support from the Ministerio de Ciencia, Innovación y Universidades (PID2021-125207NB-C32). Thanks are also given to the CTI (CSIC) for their continued computational support. M.D.G. acknowledges Universidad de Alcalá for a Starting Research Scholarship ("Ayuda de iniciación en la actividad investigadora").

Conflict of Interests

The authors declare no conflict of interests.

Data Availability Statement

Data generated or analyzed during this study are provided in full within the published article and its supplementary materials.

Keywords: hydrogen storage · ammonia borane · cyclotriborazane · pyrazole · organic catalyst

[1] I. Bhattacharjee, M. Sultana, S. Bhunya, A. Paul, *Chem. Commun.* **2022**, *58*, 1672–1684.
[2] a) C. W. Hamilton, R. T. Baker, A. Staubitz, I. Manners, *Chem. Soc. Rev.* **2009**, *38*, 279–293; b) P. G. Campbell, L. N. Zakharov, D. J. Grant, D. A. Dixon, S.-Y. Liu, *J. Am. Chem. Soc.* **2010**, *132*, 3289–3291; c) I. Alkorta, C. Trujillo, J. Elguero, M. Solimannejad, *Comput. Theor. Chem.* **2011**, *967*, 147–151.
[3] Y. Kawashima, K. Kawaguchi, E. Hirota, *J. Chem. Phys.* **1987**, *87*, 6331–6333.
[4] a) P. Paetzold, *Pure Appl. Chem.* **1991**, *63*, 345–350; b) P. Paetzold, in *Adv. Inorg. Chem., Vol. 31* (Eds.: H. J. Emeléus, A. G. Sharpe), Academic Press, **1987**, pp. 123–170.
[5] a) S. Mebs, S. Grabowsky, D. Förster, R. Kickbusch, M. Hartl, L. L. Daemen, W. Morgenroth, P. Luger, B. Paulus, D. Lentz, *J. Phys. Chem. A* **2010**, *114*, 10185–10196; b) S. J. Grabowski, *ChemPhysChem* **2014**, *15*, 2985–2993; c) S. J. Grabowski, *ChemPhysChem* **2015**, *16*, 1470–1479; d) I. Alkorta, J.

Elguero, A. Frontera, *Crystals* **2020**, *10*, 180; e) I. Alkorta, J. Elguero, J. E. Del Bene, O. Mó, M. Yáñez, *Chem. Eur. J.* **2010**, *16*, 11897–11905; f) J. E. Del Bene, I. Alkorta, J. Elguero, O. Mó, M. Yáñez, *J. Phys. Chem. A* **2010**, *114*, 12775–12779.
[6] F. H. Stephens, R. T. Baker, M. H. Matus, D. J. Grant, D. A. Dixon, *Angew. Chem. Int. Ed.* **2007**, *46*, 746–749.
[7] I. Alkorta, J. Elguero, C. Foces-Foces, *Chem. Commun.* **1996**, 1633–1634.
[8] F. Sagan, R. Filas, M. P. Mitoraj, *Crystals* **2016**, *6*, 28.
[9] P. Bhattacharya, J. A. Krause, H. Guan, *J. Am. Chem. Soc.* **2014**, *136*, 11153–11161.
[10] J. A. Buss, G. A. Edouard, C. Cheng, J. Shi, T. Agapie, *J. Am. Chem. Soc.* **2014**, *136*, 11272–11275.
[11] X. Zhang, L. Kam, T. J. Williams, *Dalton Trans.* **2016**, *45*, 7672–7677.
[12] L. Luconi, E. S. Osipova, G. Giambastiani, M. Peruzzini, A. Rossin, N. V. Belkova, O. A. Filippov, E. M. Titova, A. A. Pavlov, E. S. Shubina, *Organometallics* **2018**, *37*, 3142–3153.
[13] S. Azpeitia, C. Mendicute-Fierro, M. A. Huertos, A. Rodríguez-Diéguez, J. M. Seco, A. J. Mota, M. A. Garralda, *Eur. J. Inorg. Chem.* **2021**, *2021*, 879–891.
[14] F. H. Stephens, V. Pons, R. Tom Baker, *Dalton Trans.* **2007**, 2613–2626.
[15] Z. Lu, L. Schweighauser, H. Hausmann, H. A. Wegner, *Angew. Chem. Int. Ed.* **2015**, *54*, 15556–15559.
[16] M. Hasenbeck, J. Becker, U. Gellrich, *Angew. Chem. Int. Ed.* **2020**, *59*, 1590–1594.
[17] Y. Zhao, D. G. Truhlar, *Theor. Chem. Acc.* **2008**, *120*, 215–241.
[18] R. A. Kendall, T. H. Dunning, R. J. Harrison, *J. Chem. Phys.* **1992**, *96*, 6796–6806.
[19] M. J. Frisch, G. W. Trucks, H. B. Schlegel, G. E. Scuseria, M. A. Robb, J. R. Cheeseman, G. Scalmani, V. Barone, G. A. Petersson, H. Nakatsuji, X. Li, M. Caricato, A. V. Marenich, J. Bloino, B. G. Janesko, R. Gomperts, B. Mennucci, H. P. Hratchian, J. V. Ortiz, A. F. Izmaylov, J. L. Sonnenberg, Williams, F. Ding, F. Lipparini, F. Egidi, J. Goings, B. Peng, A. Petrone, T. Henderson, D. Ranasinghe, V. G. Zakrzewski, J. Gao, N. Rega, G. Zheng, W. Liang, M. Hada, M. Ehara, K. Toyota, R. Fukuda, J. Hasegawa, M. Ishida, T. Nakajima, Y. Honda, O. Kitao, H. Nakai, T. Vreven, K. Throssell, J. A. Montgomery Jr., J. E. Peralta, F. Ogliaro, M. J. Bearpark, J. J. Heyd, E. N. Brothers, K. N. Kudin, V. N. Staroverov, T. A. Keith, R. Kobayashi, J. Normand, K. Raghavachari, A. P. Rendell, J. C. Burant, S. S. Iyengar, J. Tomasi, M. Cossi, J. M. Millam, M. Klene, C. Adamo, R. Cammi, J. W. Ochterski, R. L. Martin, K. Morokuma, O. Farkas, J. B. Foresman, D. J. Fox, Wallingford, CT, **2016**.
[20] a) C. Appelt, J. C. Slootweg, K. Lammertsma, W. Uhl, *Angew. Chem. Int. Ed.* **2013**, *52*, 4256–4259; b) K. M. Dreux, L. E. McNamara, J. T. Kelly, A. M. Wright, N. I. Hammer, G. S. Tschumper, *J. Phys. Chem. A* **2017**, *121*, 5884–5893; c) A. Ghosh, S. Banerjee, T. Debnath, A. K. Das, *Phys. Chem. Chem. Phys.* **2022**, *24*, 4022–4041; d) I. Alkorta, J. Elguero, *Chem. Phys. Lett.* **2022**, *806*, 140051; e) A. A. Peyghan, S. A. Aslanzadeh, A. Samiei, *Monatsh. Chem.* **2014**, *145*, 1083–1087; f) A. Ghosh, T. Ash, T. Debnath, A. K. Das, *Theor. Chem. Acc.* **2018**, *137*, 116.
[21] a) C. Riplinger, F. Neese, *J. Chem. Phys.* **2013**, *138*, 034106; b) C. Riplinger, B. Sandhoefer, A. Hansen, F. Neese, *J. Chem. Phys.* **2013**, *139*, 134101; c) C. Riplinger, P. Pinski, U. Becker, E. F. Valeev, F. Neese, *J. Chem. Phys.* **2016**, *144*, 024109; d) M. Saitow, U. Becker, C. Riplinger, E. F. Valeev, F. Neese, *J. Chem. Phys.* **2017**, *146*, 164105; e) Y. Guo, C. Riplinger, U. Becker, D. G. Liakos, Y. Minenkov, L. Cavallo, F. Neese, *J. Chem. Phys.* **2018**, *148*, 011101.
[22] F. Neese, F. Wennmohs, U. Becker, C. Riplinger, *J. Chem. Phys.* **2020**, *152*, 224108.
[23] S. Mallick, B. Roy, P. Kumar, *Comput. Theor. Chem.* **2020**, *1187*, 112934.
[24] J. Tomasi, M. Persico, *Chem. Rev.* **1994**, *94*, 2027–2094.
[25] a) R. F. W. Bader, *Atoms In Molecules: A Quantum Theory*, Clarendon Pr., **1990**; b) P. L. A. Popelier, *Atoms In Molecules. An introduction*, Prentice Hall, Harlow, England, **2000**; c) C. F. Matta, R. J. Boyd, *The Quantum Theory of Atoms in Molecules: From Solid State to DNA and Drug Design*, Wiley, Weinheim, **2007**; d) Á. M. Pendás, J. Contreras-García, *Topological Approaches to the Chemical Bond*, Spinger, Switzerland, **2023**.
[26] T. A. Keith, *AIMAll (Version 11.12.19)*; TK Gristmill Software, Overland Park KS; aim.tkgristmill.com.
[27] I. Rozas, I. Alkorta, J. Elguero, *J. Am. Chem. Soc.* **2000**, *122*, 11154–11161.
[28] J. Elguero, in *Comprehensive Heterocyclic Chemistry* (Eds.: A. R. Katritzky, C. W. Rees), Pergamon, Oxford, **1984**, pp. 167–303.
[29] H. Eyring, *J. Chem. Phys.* **1935**, *3*, 107–115.
[30] a) J. Catalán, M. Menéndez, J. Elguero, *Bull. Soc. Chim. Fr.* **1985**, 30–33; b) J. Catalan, J. Elguero, in *Adv. Heterocycl. Chem., Vol. 41* (Ed.: A. R. Katritzky), Academic Press, **1987**, pp. 187–274.
[31] T. Malakar, L. Roy, A. Paul, *Chem. Eur. J.* **2013**, *19*, 5812–5817.
[32] P. W. R. Corfield, S. G. Shore, *J. Am. Chem. Soc.* **1973**, *95*, 1480–1487.
[33] D. R. Leavers, J. R. Long, S. G. Shore, W. J. Taylor, *J. Chem. Soc. A* **1969**, 1580–1581.
[34] a) R. Báez-Grez, R. Pino-Rios, *RSC Adv.* **2022**, *12*, 7906–7910; b) G. Monaco, R. Zanasi, *Phys. Chem. Chem. Phys.* **2016**, *18*, 11800–11812.
[35] H. K. Lingam, C. Wang, J. C. Gallucci, X. Chen, S. G. Shore, *Inorg. Chem.* **2012**, *51*, 13430–13436.
[36] a) I. Alkorta, J. Elguero, S. J. Grabowski, *J. Phys. Chem. A* **2008**, *112*, 2721–2727; b) S. J. Grabowski, W. A. Sokalski, J. Leszczynski, *Chem. Phys. Lett.* **2006**, *432*, 33–39; c) S. J. Grabowski, *J. Phys. Chem. A* **2007**, *111*, 3387–3393.

Manuscript received: March 26, 2023
Revised manuscript received: June 14, 2023
Accepted manuscript online: June 23, 2023
Version of record online: July 14, 2023